Composites Research

Vol. 31, No. 6, 365-370 (2018)
DOI: http://dx.doi.org/10.7234/composres.2018.31.6.365
ISSN 2288-2103(Print), ISSN 2288-2111(Online)

Paper

Effect on TENG Performance by Phase Control of TiO_x Nanoparticles

Nghia Dinh Huynh*, Hyun-Woo Park*, Kwun-Bum Chung†, Dukhyun Choi*†**

ABSTRACT: One of the critical parameters to improve the output power for triboelectric nanogenerators (TENGs) is the surface charge density. In this work, we modify the tribo-material of TENG by introducing the TiO_x embedded Polydimethylsiloxane (PDMS) in anatase and rutile phase. The effect of dielectric constant and electronic structure of the TiO_x on the capacitance of TENG and the output power as well are discussed. The surface charge density is increased as the control of the dielectric constant in difference weight percent of TiO_x and PDMS. As the results of that, the 5% TiO_x rutile phase and 7% TiO_x anatase phase embedded PDMS exhibit the highest TENG output. The peak value of voltage/current obtained from TiO_x rutile and anatase phase are ~180 V/8.2 μA and 211.6 V/8.7 μA, respectively, at the external force of 5 N and working frequency of 5 Hz, which gives over 12-fold and 15-fold power enhancement compared with the TENG based on the pristine PDMS film. This study provides a better understanding for TENG performance enhancement from the materials view.

Key Words: Triboelectric nanogenerators, TiO_x nanoparticles, Anatase phase, Rutile phase, Dielectric constant

1. INTRODUCTION

The fast economic development leading the huge energy consumption demand, as the result of that, the climate and energy crisis become a global challenge. To solve these problems, many researchers concentrate on the renewable energy generation to convert to electric power from solar, ocean waves, mechanical energies or wind power, in different power scales. While large-scale power generation is deal with megawatts of electric power, the energy harvesting devices typically concerned with smaller electric generation systems. Among them, triboelectric nanogenerators (TENGs) are the emerging technique for small-scale energy harvesting with low-cost, light-weight, high applicability and especially huge of tribo-materials choices for TENG, working by the coupling effects of static electrification and charge induction [1]. First evented in 2012 by Wang's group, TENGs basically are operated in four working modes: vertical contact-separation, in-plane contact-sliding, single-electrode, and freestanding triboelectric-layer mode [2].

The TENG output power can be significantly improved by using nano-processing for surface charge injection, the nano-patterns or surface functionalization [3]. In the contact-separation working mode, the surface charge density of the tribo-layer plays a key role to achieve high TENG output power. Polydimethylsiloxane (PDMS) is the common choice for tribo-material [4,5] thanks to its good flexibility, high electronegativity, transparency, cost less, easy to form a nano-pattern surface [6-8] or introduce an electron blocking layer between a PDMS negative tribo-material and an electrode [9] or embedded with high dielectric constant [10,11] by mixing its nanoparticles to PDMS mixture. The TENG output is sensitive to device parameters such as surface charge density, material thickness layer, dielectric constant and tribo-surface contact area or the environmental conditions as well such as humidity [12], temperature [13], the presence of ions in surrounding environment or the mechanical input force/frequency [14-16]. In the deal with surface contact area parameter, most of the previous studies investigate in different surface nanopatterning (line, cube, and pyramid type) [17]

Received 24 July 2018, received in revised form 14 November 2018, accepted 28 November 2018

*Department of Mechanical Engineering, Kyung Hee University
*†Department of Mechanical Engineering, Kyung Hee University, Corresponding author (E-mail: dchoi@khu.ac.kr)
**Department of Physics and Semiconductor Science, Dongguk University
**†Department of Physics and Semiconductor Science, Dongguk University, Corresponding author (E-mail: kbchung@dongguk.edu)

and sponge structured nanopatterning to modify the surface of tribo-material [18] in order to enhance the surface contact area leading to increase the surface charge density.

Here, we report the TiO_x nanoparticles (NPs) embedded PDMS in two different crystalline phases (anatase and rutile) based TENG structure design. The influence of TiO_x weight ratio (anatase/rutile phase) to PDMS is investigated experimentally indicate that the output power of TENG has a close relationship to the dielectric constant. The 5% rutile phase and 7% anatase phase embedded PDMS show the highest output power among all samples, which is 12-fold and 15-fold as compared to the pristine PDMS tribo-layer. Which the peak value of voltage/current obtained from TiO_x rutile and anatase phase are ~180 V/8.2 μA and 211.6 V/8.7 μA, respectively, at the 5 N external force applied and frequency of 5 Hz. Our work provides a quite straightforward to explain the electronic structure and the dielectric constant related to the TENG output performance.

2. EXPERIMENTAL

2.1 TENGs Fabrication

The schematic diagram of the proposed TENG is operated using a simple model of contact-separation mode as depicted in Fig. 1a. The TENG consists of the Aluminum (Al)/TiO_x NPs embedded PDMS at the bottom electrode and the Al electrode at the top electrode. For the bottom electrode, the PDMS solution is prepared as a mixture of base resin and curing agent (Sylgard 184A: Sylgard 184B, Dow Corning Co.) with the weight ratio of 10:1. The anatase or rutile phase of TiO_x NPs are dispersed and mixed separately into PDMS elastomer blend (with various weight ratio (wt%) of 0%, 3%, 5%, 7%, 10%, 20%, and 30%) by magnetic stirring for 15 min to obtain a uniformly mixed suspension, then degassing under vacuum for 30 min to remove the air bubbles. Afterward, the prepared TiO_x NPs/PDMS is fabricated by simple imprint lithography (SIL) technique using a doctor-blade with a 3×3 cm^2 Teflon template as a mold. Before that, the Teflon template is cleaned with acetone, ethanol, and deionized water in the ultrasonic bath in turn, and then dried by the flow of nitrogen N_2 gas. To easy peel off the PDMS composite layer from the Teflon mold, the heptadecafluoro-1, 1, 2, 2-tetrahydrodecyltrichlorosilane (HDFS) is used to modify the mold surface become hydrophobic. Next, the laminated TiO_x NPs/PDMS on Teflon template is cured at 80°C for 8 hours. Finally, the 200-μm-thick and 3×3 cm^2 PDMS embedded layer is carefully peeled off the Teflon template. Lastly, the TiO_x NPs embedded PDMS layer is attached to 3×3 cm^2 Al plate by thin PDMS solution and then cured in the oven at 100°C for 8 hours. Subsequently, to prepare the bottom electrode, the dried Al/TiO_x NPs embedded PDMS is attached to the polylactic acid (PLA) substrate by the double-side form tape.

The top electrode TENG is prepared with a 3×3 cm^2, 80 μm-thick commercial aluminum foil cleaned by ethanol and dried in N_2 gas flow. Follow that, the Al foil is attached to the PLA substrate with double-side foam tape in between.

2.2 TENGs output, electronic structure, and dielectric constant measurements

The output power of the proposed TENG with 3×3 cm^2 is measured under the vertical contact-separation mode using a pushing tester (JIPT-100, Junil Tech) to apply the external force. The TENG output voltage is measured using a Tektronix MDO3052 mixed-domain oscilloscope with an input impedance of 40 MΩ. In case of the current measurements, a Stanford Research Systems SR570 low-noise current preamplifier connected to the Tektronix MDO3052 mixed-domain oscilloscope. The TENG output power measurement is conducted at 5 Hz working frequency, 5 mm gap in between two electrodes and at the external force of 5 N. To investigate the electronic structures changing with different TiO_x anatase/rutile phase embedded PDMS, the X-ray diffraction (XRD, Bruker D5005, with Cu Kα radiation at λ = 1.541 Å) is conducted. The XAS measurements are carried out at the 2A beamline in the Pohang Accelerator Laboratory (PAL), Korea.

3. RESULTS AND DISCUSSIONS

3.1 TENG working mechanism and TiO_x Rutile-Anatase phase analysis

The designed TENG works at the contact-separation mode under the vertical pushing force as shown in Fig. 1a, consist of the Al/TiO_x NPs/PDMS at the bottom electrode and the Al on the top electrode. At the initial state, before contact of two tribo-material, there is no electrostatic potential difference across two electrodes because of no charge transfer. When they come to contact by applying the mechanical pushing force, the TiO_x NPs/PDMS film attracts the electrons from the top electrode (Al foil) to forms the negative charges on TiO_x NPs/PDMS surface, and induce the positive charges on the Al top electrode. During the periodic external force applied, the triboelectric charges on the PDMS surface leading to a periodic movement of electrons between the top and bottom electrodes for generating the electron flows, or electric current in the external circuit.

Basically, the TiO_x has three different crystal structures: rutile, anatase, and brookite. Each crystal structure affects their physical properties, optical, electrical. To determine the size of TiO_x NPs in anatase and rutile phase that used in this study, we investigate the XRD patterns analysis as depicted in Fig. 1b-c. As shown in the XRD graph, the typical polycrystalline anatase phase, the typical polycrystalline structure with the diffraction peaks of (101), (103), (004), (112), (200), (105), (211), (204), (116), (220), and (215). The calculated particle size of anatase phase is 22.4 nm by the main peak of (101) follow the Scherrer's formula can be expressed as:

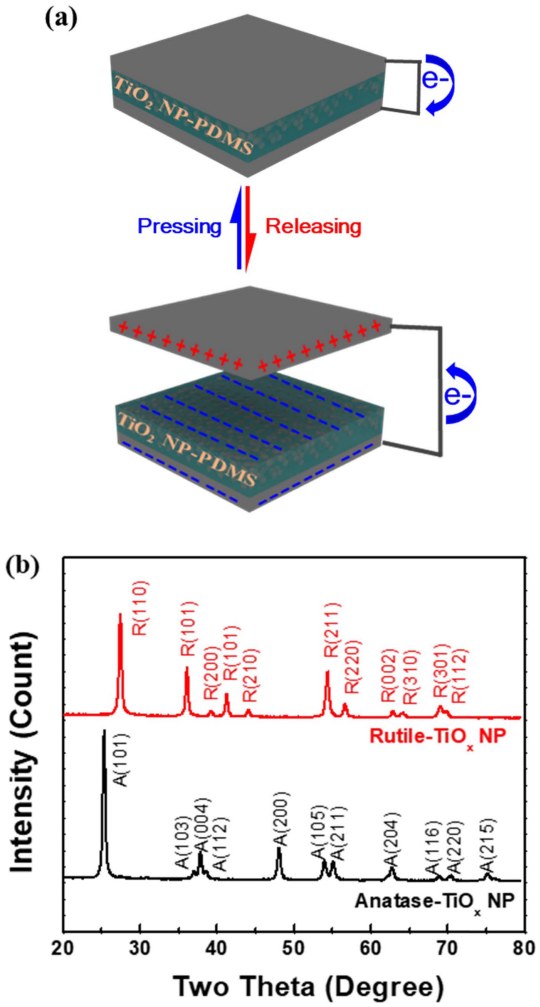

Fig. 1. (a) Experimental design for TiO_x NPs embedded PDMS based TENG, (b) XRD analysis of TiO_x NPs Anatase and Rutile phase

$$D_p = K\lambda/(B\times\cos\theta)$$

Where:

D_p : Average crystallite size (nm)
K : Scherrer constant. K varies from 0.68 to 2.08; K = 0.94 for spherical crystallites with cubic symmetry
λ : X-ray wavelength. For mini XRD, Cu Kα average = 1.54178 Å
B : Full Width at Half Maximum) of XRD peak
θ : XRD peak position, one half of 2θ

In case of the rutile structure with the diffraction peaks of (110), (101), (200), (101), (210), (211), (220), (002), (310), (301), and (112), and the calculated particle size of rutile phase is 20.35 nm through main XRD peak of (110).

3.2 TENGs output power

The output voltage and current of the TiO_x NPs/PDMS based TENG at different weight ratio compared to the pristine PDMS based TENG are shown in Fig. 2a-b (rutile phase) and Fig. 2c-d (anatase phase). All TENG devices are measured at the same surrounding condition of ~65% relative humidity, the temperature of 27°C and the external force is maintained constantly at 5 N, external pushing frequency of 5 Hz, and the gap in between top and bottom triboelectric layers is 5 mm. The output voltage and current plot generated by the TENG device linearly increase from 0% (pristine) to 5% of rutile TiO_x NPs/PDMS as shown in Fig. 2a-b, respectively. The TENG with pristine PDMS layer produce the output voltage and current values of ~77.3 V and ~1.6 μA, respectively, when the pristine PDMS and Al electrode at the top side are brought into contact and separation. By introducing 3% and 5% of rutile TiO_x NPs/PDMS, the output voltage and current values of the TENG devices are further enhanced. This output improvement mainly due to the enhancement of the dielectric constant and its electronic structure. The optimal output voltage and current values are ~180 V and ~8.2 μA, determined by the 5% of rutile TiO_x NPs/PDMS.

As the result of the optimal rutile TiO_x NPs/PDMS, the TENG output power is increased ~12 times as compared to the pristine PDMS based TENG. In contrast, as the wt% of rutile TiO_x NPs/PDMS increased more than 5%, the TENG output voltage and current decreased linearly to ~38.7 V and ~1.5 μA, respectively, which are almost a half of the pristine TENG voltage output. Meanwhile, the anatase phase of TiO_x NPs/PDMS based TENG also exhibit the same trend of the output voltage and current as the rutile phase.

As the anatase weight ratio of TiO_x NPs/PDMS increase from 0% (pristine PDMS based TENG) to 7%, the output voltage and current characteristics are significantly increased from ~77.3 V and ~1.6 μA to ~211.7 V and ~8.7 μA, respectively. By that, the output power of the optimal anatase TiO_x NPs/PDMS based TENG is about 15 times as compared to the pristine PDMS TENG. However, at the higher weight ratio than 7% TiO_x NPs/PDMS, the output voltage and current significantly decreases to ~104 V and ~4 μA, respectively.

3.3 Electronic Structure and dielectric constant analysis

As the dielectric material filled into PDMS, the dielectric constant of the embedded PDMS layer is changed. To increase the dielectric constant of the PDMS layer, the high dielectric constant material TiO_x NPs is used to disperse to the PDMS solution to form the composite PDMS tribo-layer. Here, we fill the rutile and anatase phase of TiO_x NPs into PDMS to modify its dielectric constant. Fig. 3 shows the dielectric constant linearly changes as a function of rutile and anatase TiO_x NPs embedded PDMS in different weight ratio to form the 200-μm-thick PDMS embedded layer. The measured dielectric constant of the rutile and anatase TiO_x NPs embedded PDMs are linearly increased as the increase of the weight ratio filling. However, more than 5% of rutile mixture PDMS, the TENG

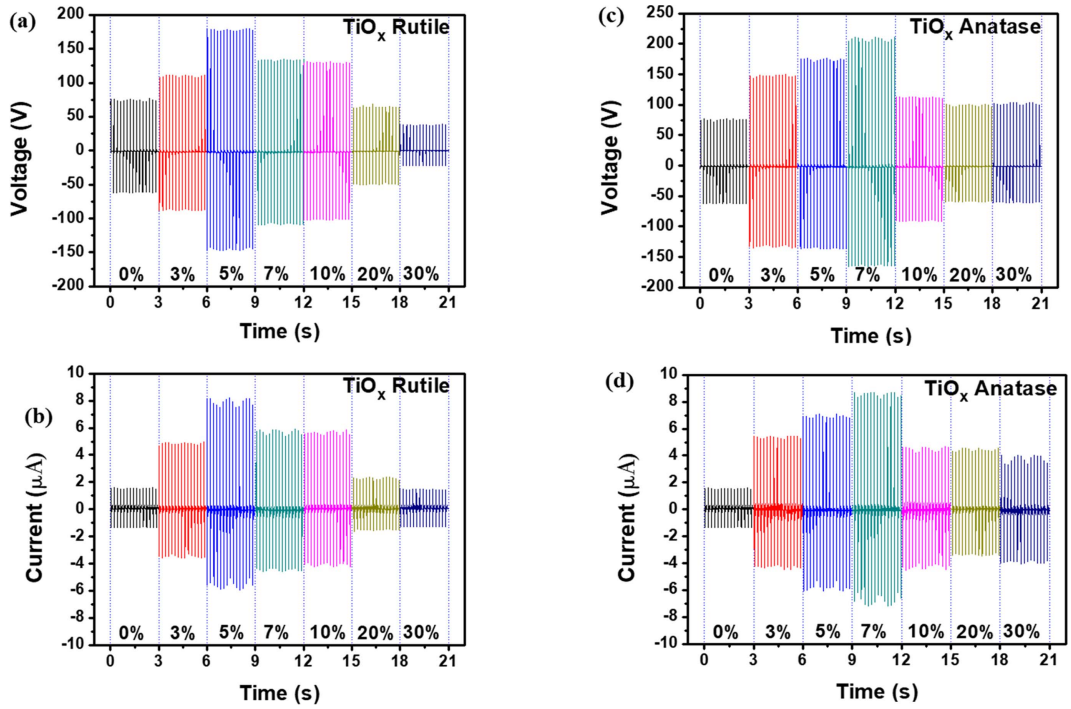

Fig. 2. The effect various TiO_x NPs embedded PDMS composition in (a)-(b) rutile and (c)-(d) anatase phase as a function of the TENG output voltage and current

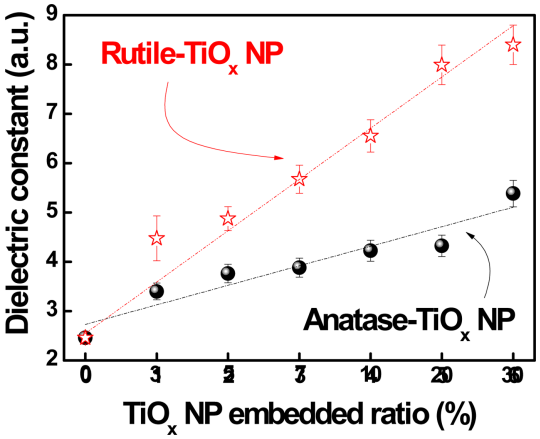

Fig. 3. Dielectric constant linearly changes as a function of TiO_x NPs embedded PDMS weight ratio from 0% to 30% wt % in rutile and anatase phase

output power dramatically decrease. For anatase mixture PDMS, the optimal is 7% weight ratio, more than that the output performance of TENG is also dropped. The values of the dielectric constant of different embedded concentrations are shown in Table 1.

In order to explain the root cause of the phenomenon that the TENG output does not linearly increase with the weight ratio increase, especially at more than 5% rutile and 7% anatase mixed PDMS, the correlation between the electronic structures of the TiO_x NPs embedded PDMS and the energy

Table 1. Dielectric constant of different wt% of rutile and anatase TiO_x NPs embedded PDMS

TiO_2 embedded concentrations (%)	Rutile	Anatase
0%	2.46	
3%	4.48	3.40
5%	4.88	3.76
7%	5.67	3.88
10%	6.55	4.23
20%	7.99	4.32
30%	8.4	5.38

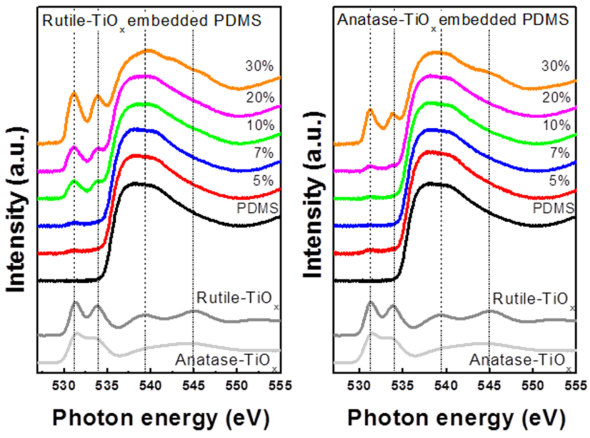

Fig. 4. O-K edge XAS spectra of PDMS layers as a function of the TiO_x NPs embedded PDMS by weight ratio

conversion mechanism of TENG is presented. Fig. 4 shows the normalized O-K edge XAS spectrum of the TiO_x NPs embedded PDMS layer with respect to embed ratio of each TiO_x NPs (rutile and anatase). In addition, we co-plot the O-K edge XAS spectrum of each TiO_x NPs (gray lines) for easy comparison with the changes in the TiO_x NPs embedded PDMS. As the increased weight ratio of TiO_x NPs from 0 to 30%, the electronic structure of PDMS is apparently changed by the addition of the electronic structure of TiO_x NPs, regardless of the phase of NPs. These changes in the tribo-material surface can cause changes in the tribo-series, resulting in reduced tribo-electrification effects. However, rutile TiO_x embedded PDMS has strong surface changes at same embedded ratio compared to anatase TiO_x embedded PDMS.

This means that rutile-TiO_x embedded PDMS can induce large changes in tribo-series even at small doping concentrations compared to anatase-TiO_x embedded PDMS.

4. CONCLUSIONS

In summary, we introduced the simple method to enhance the output performance of TENGs by high dielectric TiO_x NPs embedded into the PDMS composite layer. Here, we find the optimal 5% rutile and 7% anatase phase of TiO_x NPs when filling to the PDMS. The rutile 5% shows the highest output voltage and current of ~180 V and ~8.2 μA, respectively, among another rutile weight ratio. In case of the anatase, the 7% weight ratio exhibits the greatest output voltage and current of ~211.7 V and ~8.7 μA, respectively. The TENG output improvement is strongly relating to the enhancement of the dielectric constant of the tribo-material. However, at TiO_x NPs embed over 5% in rutile and over 7% in anatase phase, the output voltage and current are dropped dramatically to ~38.7 V/~1.5 μA (rutile 30%) and ~104 V/~4 μA, respectively.

ACKNOWLEDGMENT

This work was supported by the National Research Foundation of Korea (NRF) Grant funded by the Korea government (MSIP) (No.2016R1A4A1012950), (No. 2017R1D1A1B03032375), and (No. 2017R1A6A3A11029892).

REFERENCES

1. Zhu, G., Peng, B., Chen, J., Jing, Q., and Wang, Z.L., "Triboelectric Nanogenerators as a New Energy Technology: From Fundamentals, Devices, to Applications," *Nano Energy*, Vol. 14, 2015, pp. 126-138.
2. Wang, Z.L., "On Maxwell's Displacement Current for Energy and Sensors: the Origin of Nanogenerators," *Materials Today*, Vol. 20, No. 2, 2017, pp. 74-82.
3. Byun, K.E., Cho, Y., Seol, M., Kim, S., Kim, S.W., Shin, H.J., Park, S., and Hwang, S., "Control of Triboelectrification by Engineering Surface Dipole and Surface Electronic State," *ACS Applied Materials & Interfaces*, Vol. 8, No. 28, 2016, pp. 18519-18525.
4. He, X., Guo, H., Yue, X., Gao, J., Xi, Y., and Hu, C., "Improving Energy Conversion Efficiency for Triboelectric Nanogenerator with Capacitor Structure by Maximizing Surface Charge Density," *Nanoscale*, Vol. 7, No. 5, 2015, pp. 1896-1903.
5. Chen, J., Guo, H., He, X., Liu, G., Xi, Y., Shi, H., and Hu, C., "Enhancing Performance of Triboelectric Nanogenerator by Filling High Dielectric Nanoparticles into Sponge PDMS Film," *ACS Applied Materials & Interfaces*, Vol. 8, No. 1, 2015, pp. 736-744.
6. Dudem, B., Huynh, N.D., Kim, W., Kim, D.H., Hwang, H.J., Choi, D., and Yu, J.S., "Nanopillar-array Architectured PDMS-Based Triboelectric Nanogenerator Integrated with a Windmill Model for Effective Wind Energy Harvesting," *Nano Energy*, Vol. 42, 2017, pp. 269-281.
7. Lee, K.Y., Chun, J., Lee, J.H., Kim, K.N., Kang, N.R., Kim, J.Y., Kim, M.H., Shin, K.S., Gupta, M.K., Baik, J.M., and Kim, S.W., "Hydrophobic Sponge Structure-based Triboelectric Nanogenerator," *Advanced Materials*, Vol. 26, No. 29, 2014, pp. 5037-5042.
8. Jeong, C.K., Baek, K.M., Niu, S., Nam, T.W., Hur, Y.H., Park, D.Y., Hwang, G.T., Byun, M., Wang, Z.L., Jung, Y.S., and Lee, K.J., "Topographically-designed Triboelectric Nanogenerator via Block Copolymer Self-assembly", *Nano Letters*, Vol. 14, No. 12, 2014, pp. 7031-7038.
9. Park, H.W., Huynh, N.D., Kim, W., Lee, C., Nam, Y., Lee, S., Chung, K.B., and Choi, D., "Electron Blocking Layer-based Interfacial Design for Highly-enhanced Triboelectric Nanogenerators," *Nano Energy*, Vol. 50, 2018, pp. 9-15.
10. Park, K.I., Lee, M., Liu, Y., Moon, S., Hwang, G.T., Zhu, G., Kim, J.E., Kim, S.O., Kim, D.K., Wang, Z.L., and Lemke, K.J., "Flexible Nanocomposite Generator Made of $BaTiO_3$ Nanoparticles and Graphitic Carbons," *Advanced Materials*, Vol. 24, No. 22, 2012, pp. 2999-3004.
11. Sun, H., Tian, H., Yang, Y., Xie, D., Zhang, Y.C., Liu, X., Ma, S., Zhao, H.M., and Ren, T.L., "A Novel Flexible Nanogenerator Made of ZnO Nanoparticles and Multiwall Carbon Nanotube," *Nanoscale*, Vol. 5, No. 13, 2013, pp. 6117-6123.
12. Nguyen, V., and Yang, R., "Effect of Humidity and Pressure on the Triboelectric Nanogenerator," *Nano Energy*, Vol. 2, No. 5, 2013, pp. 604-608.
13. Lu, C.X., Han, C.B., Gu, G.Q., Chen, J., Yang, Z.W., Jiang, T., He, C., and Wang, Z.L., "Temperature Effect on Performance of Triboelectric Nanogenerator," *Advanced Engineering Materials*, Vol. 19, No. 12, 2017, p. 1700275.
14. Kim, W., Hwang, H.J., Bhatia, D., Lee, Y., Baik, J.M., and Choi, D., "Kinematic Design for High Performance Triboelectric Nanogenerators with Enhanced Working Frequency," *Nano Energy*, Vol. 21, 2016, pp. 19-25.
15. Bhatia, D., Kim, W., Lee, S., Kim, S.W., and Choi, D., "Tandem Triboelectric Nanogenerators for Optimally Scavenging Mechanical Energy with Broadband Vibration Frequencies," *Nano Energy*, Vol. 33, 2017, pp. 515-521.

16. Bhatia, D., Lee, J., Hwang, H.J., Baik, J.M., Kim, S., and Choi, D., "Design of Mechanical Frequency Regulator for Predictable Uniform Power from tribOelectric Nanogenerators," *Advanced Energy Materials*, Vol. 8, No. 15, 2018, p. 1702667.
17. Fan, F.R., Lin, L., Zhu, G., Wu, W., Zhang, R., and Wang, Z.L., "Transparent Triboelectric Nanogenerators and Self-powered Pressure Sensors Based on Micropatterned Plastic Films," *Nano Letters*, Vol. 12, No. 6, 2012, pp. 3109-3114.
18. Lee, K.Y., Chun, J., Lee, J.H., Kim, K.N., Kang, N.R., Kim, J.Y., Kim, M.H., Shin, K.S., Gupta, M.K., Baik, J.M., and Kim, S.W., "Hydrophobic Sponge Structure-based Triboelectric Nanogenerator," *Advanced Materials*, Vol. 26, No. 29, 2014, pp. 5037-5042.